

Modifying a commonly expressed endocytic receptor retargets nanoparticles *in vivo*

Figure S1. **(a)** QUANT Barcode Design. **(b)** Comparison of Mean Fluorescent Intensity (MFI) of barcodes conjugated with Alexa-488 and Alexa-647 at 200ng and 50ng per well. * $p<0.05$, *** $p<0.001$, 2 tailed t-test. **(c)** Cell types in the liver, heart, lung, spleen, and kidney were sorted based on the following FACS Markers. **(d)** Representative FACS gating for lung. We isolated endothelial cell ($CD31^+CD45^-$) and macrophages ($CD31^-CD45^+CD11b^+$). **(e)** Representative FACS gating for liver. We isolated endothelial cells ($CD31^+CD45^-$), Kupffer cells ($CD31^-CD45^+CD68^+$), and Hepatocytes ($CD31^-CD45^-CD68^-$). **(f)** MFI of barcodes conjugated with Alexa-647 in wild-type and Cav1^{-/-} mice.

a

G*A*T*GCTCTACGAACTCGTCCNHNWCTGCTAGTCCACGTCCATGTCCACCWNHNT**GATATTG**NWH**GTGGTTAGTCGAGCAGAGAC*T*A*G**

Red = phosphorothioate linkages (*) act to increase resistance to exonucleases.

Green = Universal primer binding sites allow for amplification from cells/tissues and linkage to next generation sequence adapters

Blue = Probe binding site. This functionality is used in ddPCR

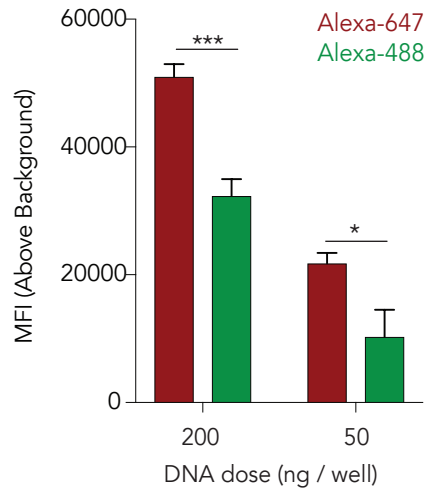
Orange = 8nt Barcode. This 8nt sequence is referenced to identify nanoparticle composition and track nanoparticle distribution.

Light Blue = 4nt placed used to prevent steric blocking of universal forward primer and probe in ddPCR.

Black = Random nucleotide region used to minimize PCR bias.

N= A, T, G, or C; W= A or T; H= A, T, or C.

b



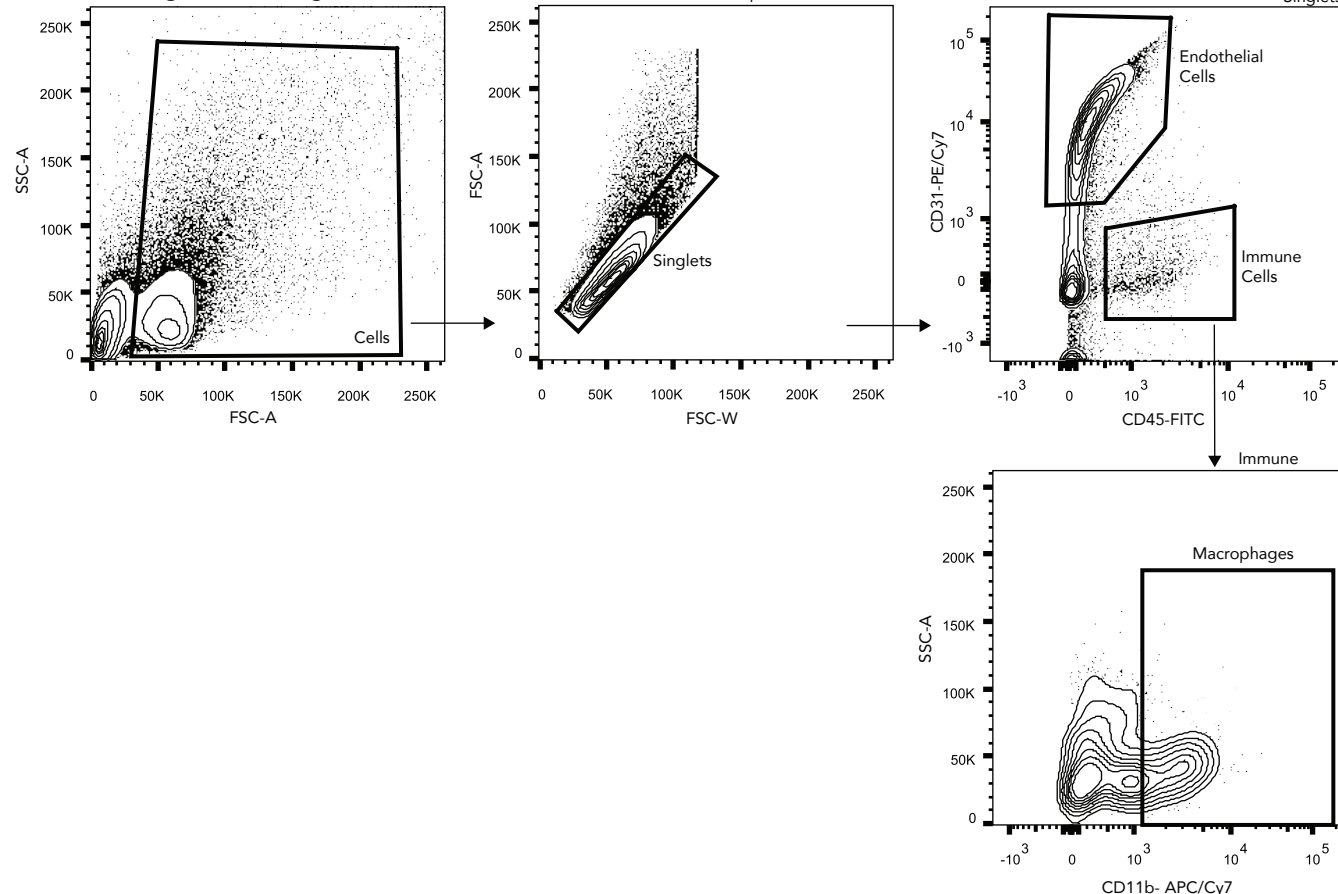
c

Cell Type	FACS Markers	Tissue
B cells	CD3- CD19+	S
T cells	CD19- CD3+	S
Macrophages	CD31- CD45+ CD11b+	L,K
Kupffer Cells	CD31- CD45+ CD68+	v
Endothelial cells	CD31+ CD45-	v,H,L,K
Immune	CD31- CD45+ CD11b-	v,L,K
Hepatocytes	CD31- CD45-	v

Liver, Heart, Lung, Spleen, Kidney

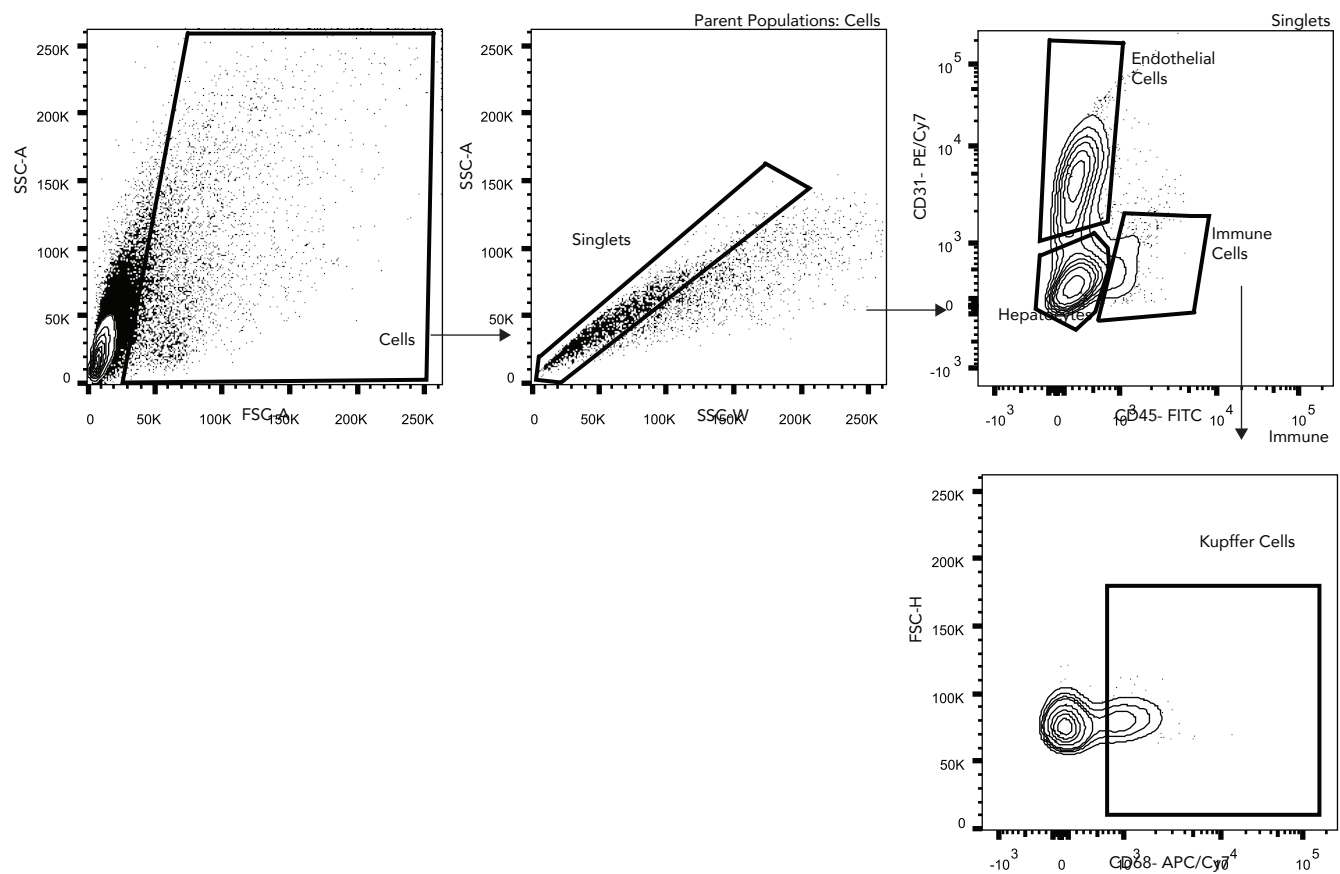
d

Representative Lung FACS Gating



e

Representative Liver FACS Gating



f

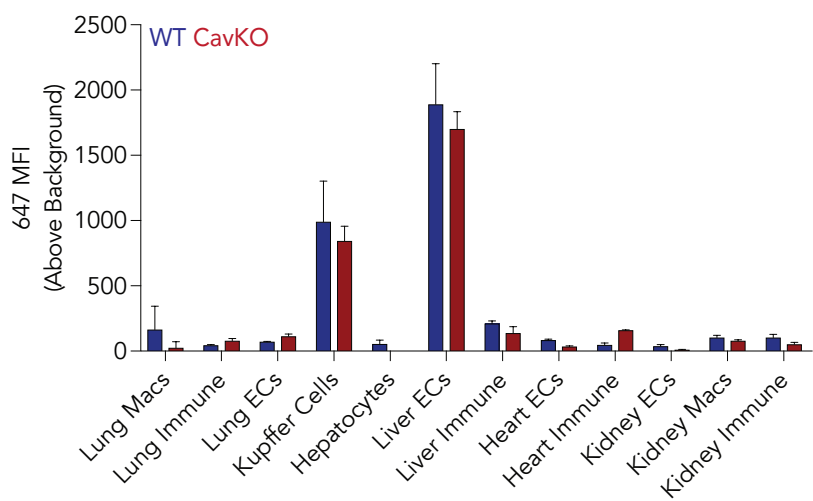
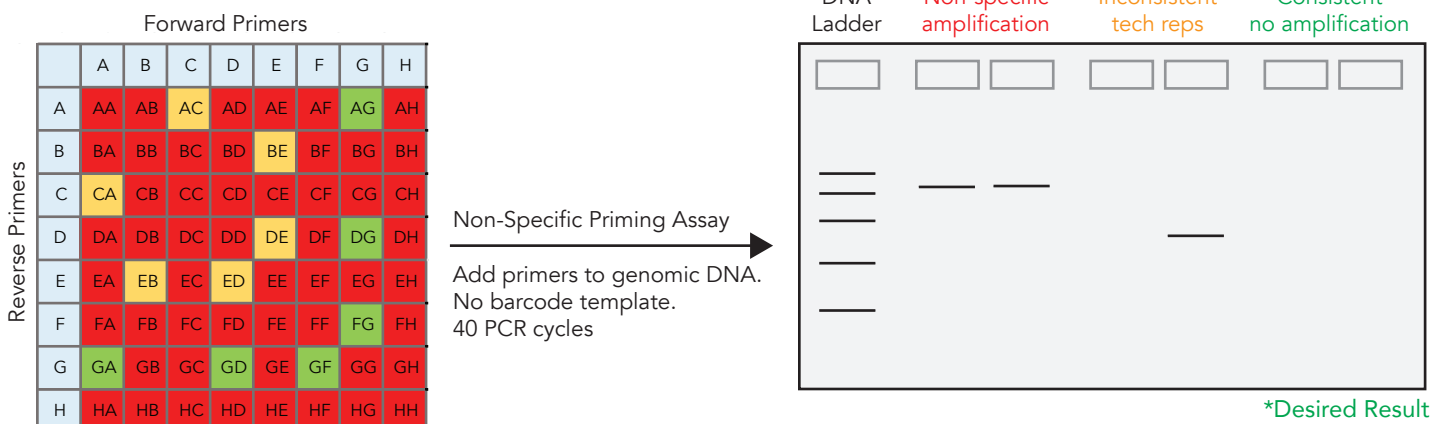


Figure S2. A multi-step approach to optimizing the signal generated by ddPCR QUANT barcodes. **(a)** Primer combinations were tested to avoid non-specific amplification by genomic DNA (gDNA). Different primer pairs were added to mouse and human gDNA without any barcode template. **(b)** Primers that did not amplify gDNA were selected. **(c)** A two-step PCR adds Illumina nextera chemistry regions, indices, and Illumina adapters for Illumina sequencing and **(d)** produces a clear product. **(e)** Dual indices allow for multiplexed Illumina sequencing. **(f)** ddPCR was optimized using an annealing temperature of 60°C and **(g)** probe concentration 2x more than the ddPCR standard protocol concentration. **(h)** A scrabbled probe site was tested to verify the specificity of the probe-based signal.

a



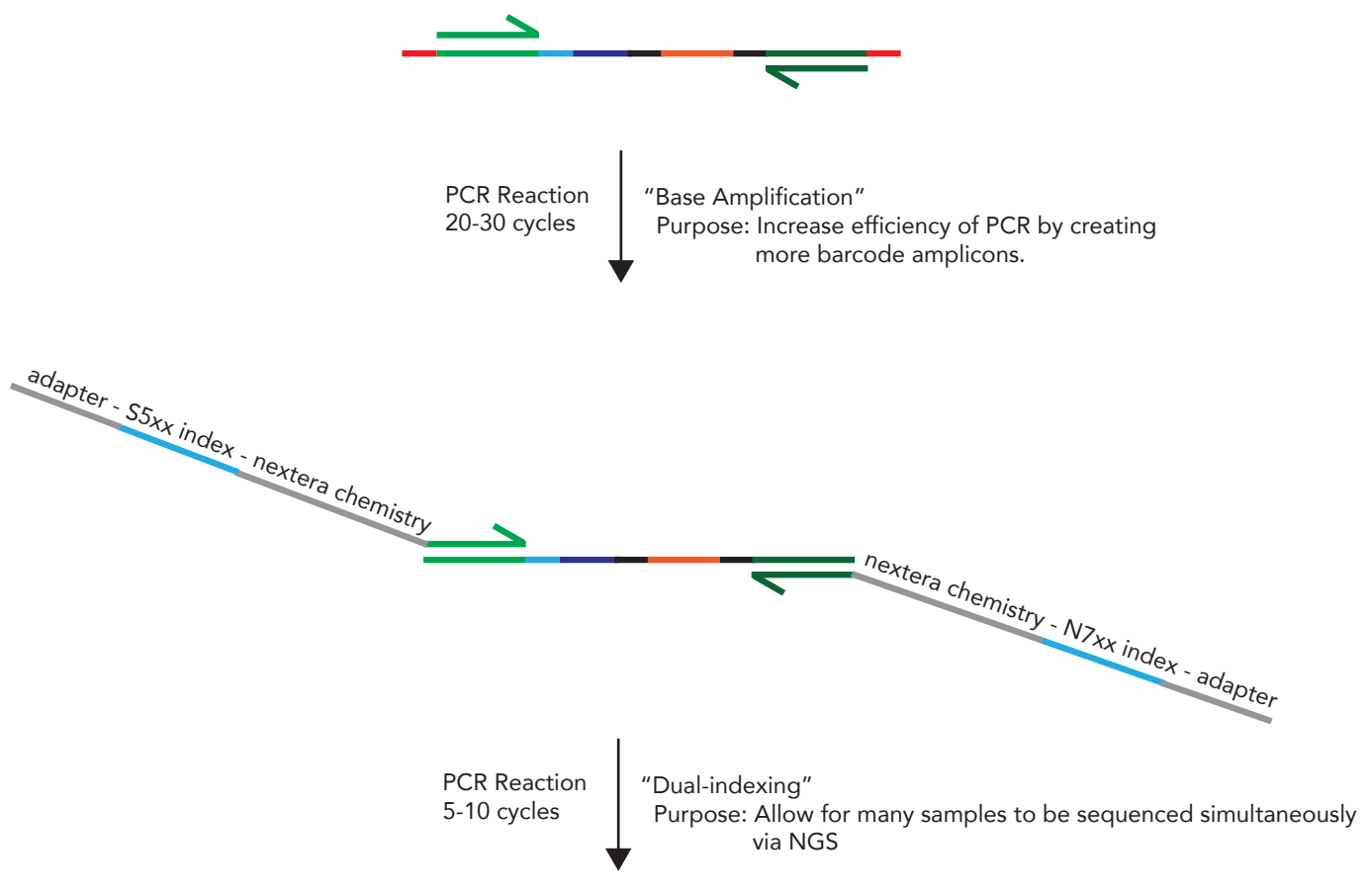
b

A	GCACGCCCTTACGACTCATCT
B	GCTCAATACTGTTCCACCGC
C	ACTCACTTCGCATTAGCCGC
D	GCTCTCATACGAACCTCGTCC
E	GCACACCGCTTCTGAATCT
F	ATCTCTCGCACTCTAACGG
G	GTCTCTGCTCGACTAACACCAC
H	ATCACTCCGCACCGCTTATG

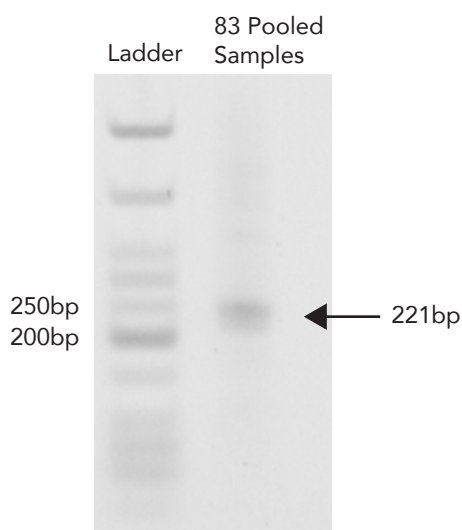
Forward Primer

Reverse Primer

c



d

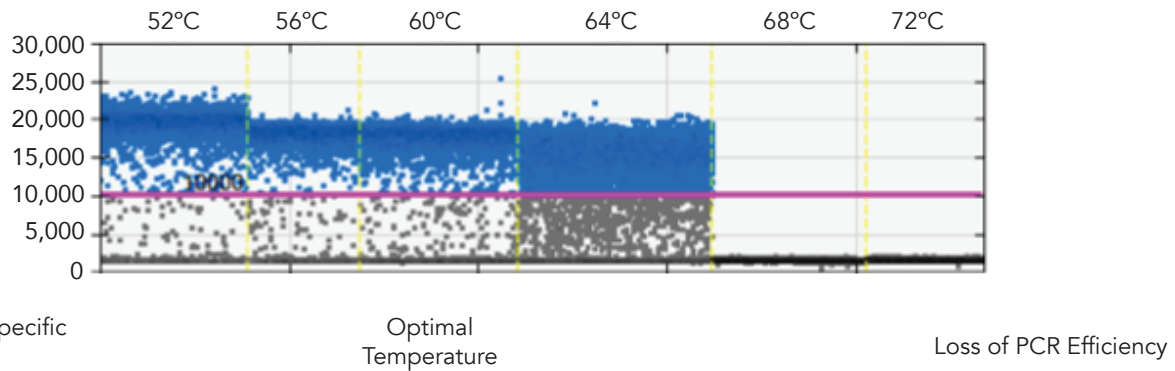


e

N701	TCGCCTTA	S502	CTCTCTAT
N702	CTAGTACG	S503	TATCCTCT
N703	TTCTGCCT	S505	GTAAGGAG
N704	GCTCAGGA	S506	ACTGCATA
N705	AGGAGTCC	S507	AAGGAGTA
N706	CATGCCTA	S508	CTAACGCCT
N707	GTAGAGAG	S510	CGTCTAAT
N710	CAGCCTCG	S511	TCTCTCCG
N711	TGCCTCTT	S513	TCGACTAG
N712	TCCTCTAC	S515	TTCTAGCT
N714	TCATGAGC	S516	CCTAGAGT
N715	CCTGAGAT	S517	GCGTAAGA
N716	TAGCGAGT		
N718	GTAGCTCC		
N719	TACTACGC		
N720	AGGCTCCG		

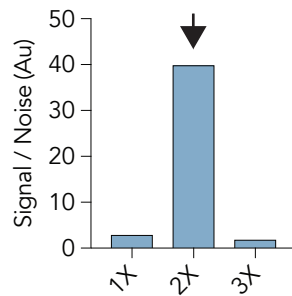
f

Annealing/Extension Temp.
Optimization



g

Probe Concentration Optimization



h

Scrambled Probe Site: 5'- ACCAACGCCGTATCCGTCCCTTCCG -3'
Correct Probe Site: 5'- CCTGCTAGTCCACGTCCATGTCCACC -3'

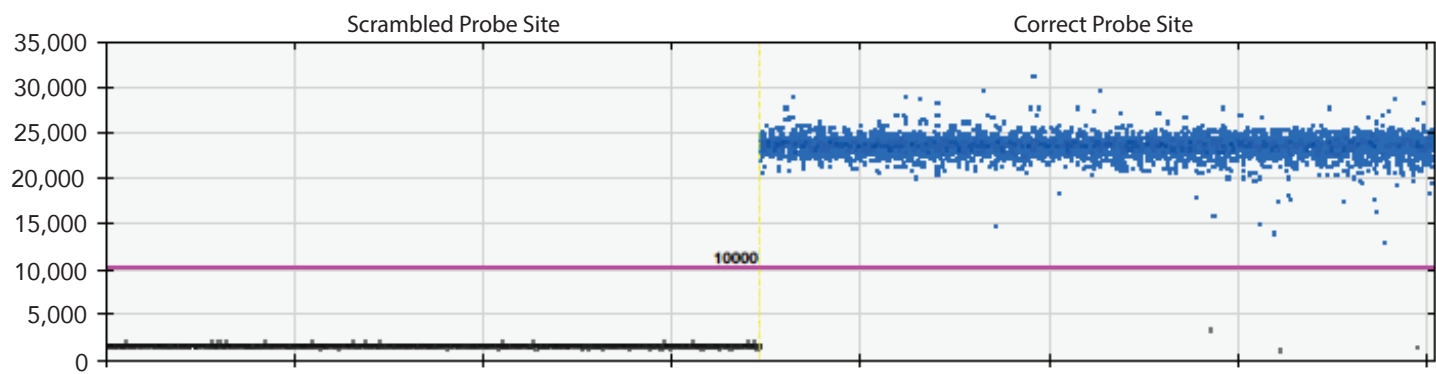


Figure S3. (a) Alexa-647 fluorescence 24 hours after fluorescently labeled QUANT barcodes were administered *in vitro* to iMAECs with Lipofectamine 2000 and analyzed with flow cytometry.

a

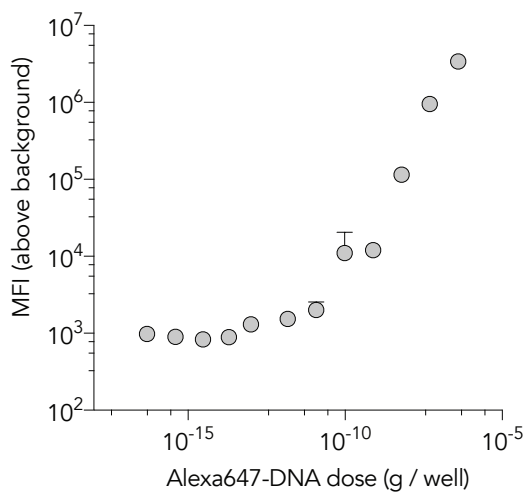
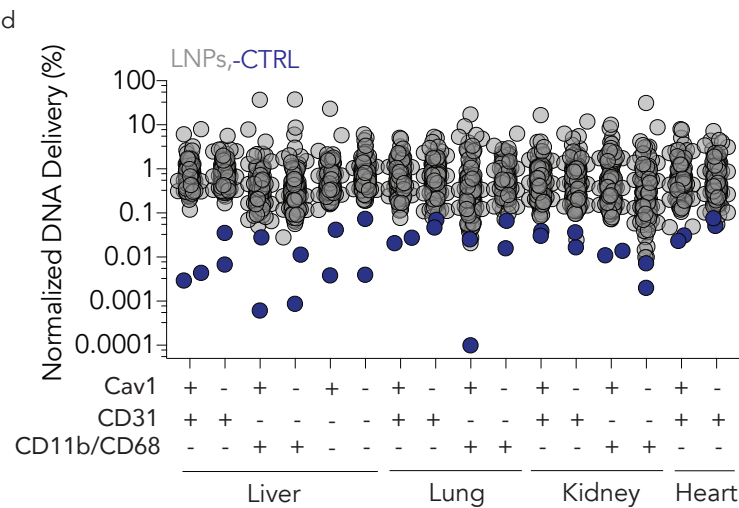
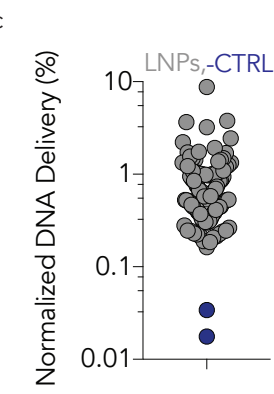
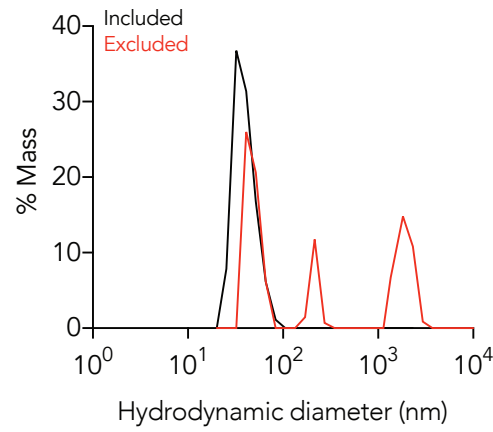
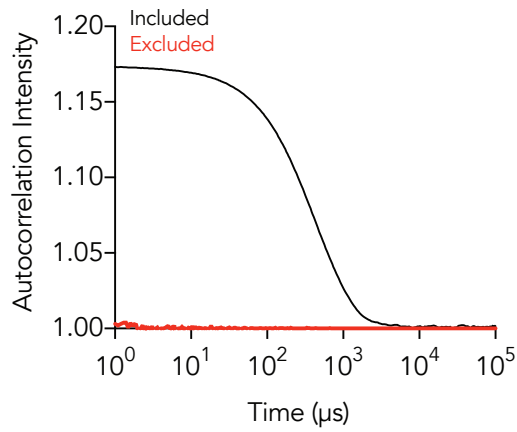


Figure S4. (a) 156 8-nucleotide barcodes sequences were rationally selected for their ability to be multiplexed on Illumina Miniseq Machines. (b) Using dynamic light scattering (DLS), LNPs were included if they met the following inclusion criteria: autocorrelation curves with 1 inflection point and hydrodynamic diameters between 20 nm and 200 nm. (c) Average normalized delivery of each LNP from library 2. (d) In all samples of library 2, naked barcode – the negative control – was delivered less efficiently than barcodes carried by LNPs, as expected. (e) The following example illustrates how our deep sequencing data was normalized. (f) Cells were sorted on the indicated FACS markers. (g) LNPs libraries for screens 1 and 2 were synthesized with the LNP 7C1, Cholesterol, DSPC, and variable PEG compounds at variable molar ratios. (h) The formulation ratios and diameter of each LNP for screen 1. (i) Nanoparticle formulation ratios for screen 2; in this screen, we formulated 120 different LNPs. (j) Stable LNPs with diameters between 20 and 200 nm were included. (k) The formulation ratios and diameter of each LNP for screen 2.

a

G*A*T*GCTCTACGAACTCGTCCNHNWCCTGCTAGTCCACGTCCATGTCCACCNWNH-8nt Barcode Seq-NWHGTGGTTAGTCGAGCAGAGAC*T*A*G

BC #	Seq	BC #	Seq	BC #	Seq	BC #	Seq
1	TGATATTG	40	TCTAACTG	79	ATCAATTG	118	CGCTTAAC
2	GACGCAAT	41	TATGCCCT	80	GGTCGGTC	119	CTGACCGC
3	GCGAGTAT	42	GTAATTGC	81	TTGGATCC	120	TGACCAGG
4	ACCTAAC	43	GTCTCCGT	82	ATTGGTTC	121	CTCATAGG
5	AGGCGCTA	44	TGCATGGT	83	GATGGCCT	122	CCGTAAGC
6	GATCTACC	45	AGTCCGGT	84	TTATAGCA	123	CGAGACGT
7	CTACTGAT	46	TCCTGATG	85	GTCAATCT	124	GACGATAA
8	TGATCTAT	47	ATCGTCTA	86	CGCTCCGG	125	CCGCTGCT
9	ATGAGATG	48	GGACGTCC	87	ACTCAAGT	126	GGTTAGAA
10	GCGAATT	49	CTACGAGG	88	CCGTTCCG	127	TTATCCGG
11	GATTCCGG	50	CAATCCGT	89	CCGCAGAG	128	AGTAGGTA
12	ATAATATA	51	GGCGCTTG	90	CGGTATCT	129	CGTACTAC
13	AGCATGCG	52	GTCCGTTA	91	TTATTAAT	130	AACTAGCG
14	GATTCAAC	53	GCCTCTCG	92	AGGCTCAT	131	TGCTCCTT
15	TACCTGCT	54	GAGAGTTG	93	TAGTACGT	132	TCGCCAAC
16	GCTAATCG	55	CATAATAG	94	AATATACG	133	CGCGGCTC
17	CTCCTTCG	56	TCTAGAGT	95	CGATGCTT	134	AAGGCGGT
18	ACGCTAGC	57	AAGTCTAG	96	CCAAGATT	135	GTAATGAG
19	GCAGGACT	58	ATTCGAGA	97	TCCATTAT	136	AGATACTA
20	ATTGCTCT	59	CTACCATT	98	AATACCAT	137	GAATCGTC
21	TACGCTCG	60	GTTAGTCA	99	CTGCGACC	138	AGGAAGAG
22	ACGCTCCA	61	ATAGAAC	100	GACTTGAG	139	CAGGTACC
23	CGGTCAT	62	CTCAACTA	101	CAGAACGCA	140	TAGATAGC
24	CGCCTATT	63	CTTACGTC	102	TCTCCTAA	141	AGAGTAAG
25	TTGCGTTG	64	TGAGTTCG	103	CTGAGCCA	142	TCATTCCG
26	TCCTAAGA	65	ATGGTAGA	104	TCCTGCGC	143	CGGCGTCG
27	CAAGAAGG	66	TCCAGGCG	105	CGAACGCC	144	ATCAAGCA
28	TAGAATT	67	CTCAGCAT	106	CTGCTCTA	145	TTGGCGTA
29	GGCGCCAA	68	TGCGTATA	107	GCCTACCA	146	CGTCGGCA
30	TAGATCCG	69	AATGCTAC	108	GGATGAAG	147	AGGACCGA
31	CGAGCAGC	70	CGCGAGGC	109	CTATATAC	148	CCTCGATC
32	TAAGATGA	71	GTCGAAGT	110	CGAATATG	149	TATCTGAG
33	AGCTCGGA	72	ACTATCTC	111	ACGCATTA	150	CGGAGTAA
34	TAACCGAA	73	GTCGCCTC	112	GGTAGACC	151	AGAATGAA
35	TATATCTA	74	AGTTACCG	113	CGTTATGC	152	AATCGGTT
36	AAGAGGAT	75	GAGTATAC	114	TCTGCGGA	153	CATCGCCA
37	ACGTCGAA	76	GGCAGTAG	115	CCTTGCAT	154	TATTGACT
38	CATCATTA	77	TGGAGACG	116	ATTATAGT	155	GTAGGCAG
39	TTGCAACT	78	ATTAGGAC	117	CTCGTAAT	156	GTTCGTAT



e

		Raw Counts Lung Endothelial Cells			Raw Counts Kidney Endothelial Cells			
LNP	Barcode	Mouse 1	Mouse 2	Mouse 3	Mouse 1	Mouse 2	Mouse 3	Input
1	GACACAGT	100	80	200	300	200	250	100
2	GCATAACG	50	45	110	100	60	70	120
3	ACAGAGGT	120	105	250	150	90	110	110
Total Counts		270	230	560	550	350	430	330

		Normalized Counts Lung ECs (%)			Normalized Counts Kidney ECs (%)			
LNP	Barcode	Mouse 1	Mouse 2	Mouse 3	Mouse 1	Mouse 2	Mouse 3	Input
1	GACACAGT	37	35	36	55	57	58	30
2	GCATAACG	19	20	20	18	17	16	36
3	ACAGAGGT	44	46	45	27	26	26	33
Total (%)		100	100	100	100	100	100	100

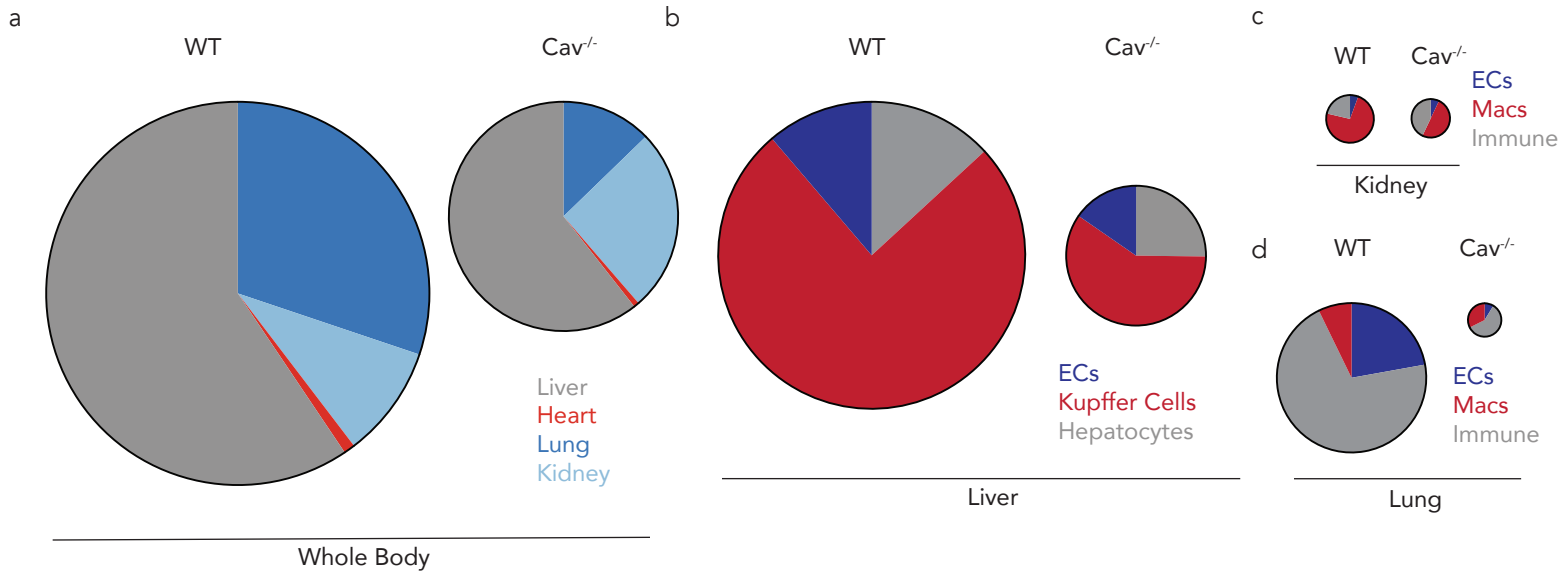
		Normalized to input Counts Lung ECs (%)			Normalized to input Counts Kidney ECs (%)			
LNP	Barcode	Mouse 1	Mouse 2	Mouse 3	Mouse 1	Mouse 2	Mouse 3	
1	GACACAGT	40	38	39	58	60	61	
2	GCATAACG	17	18	18	16	15	14	
3	ACAGAGGT	44	45	44	26	25	24	
Total (%)		100	100	100	100	100	100	

f

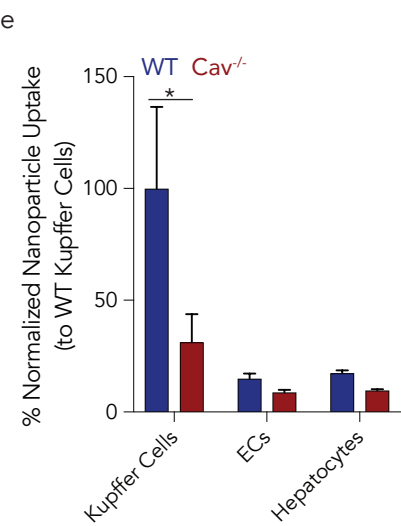
Cell Type	FACS Markers	Tissue
Endothelial cells	CD31+ CD45-	v, H, L, K
Macrophages	CD31-CD45+CD11b+	L,K
Kupffer Cells	CD31- CD45+ CD68+	v
Immune Cells	CD31- CD45+ CD11b-	L,K
Hepatocytes	CD31- CD45- CD68-	v

Liver, Heart, Lung, Kidney

Figure S5. **(a)** Total ddPCR barcode counts for library 2 – equal to the area of the circle - were used to determine the overall biodistribution from the LNP screens previously described across multiple organs from wild-type and Cav1^{-/-} mice. **(b)** The total ddPCR counts were determined in different cell-types from the liver, **(c)** lung and **(d)** kidney. **(e)** Within the liver cell-types, normalized nanoparticle biodistribution demonstrates that Kupffer cells in Cav1^{-/-} uptake less nucleic acids when compared to Kupffer cells from wild-type mice. *p<0.05 2-way ANOVA. **(f)** Combined sequencing data and ddPCR results shows the absolute delivery of 115 nanoparticles for each LNP in the liver in wild type (blue) and Cav1^{-/-} (red) mice, from library 1, in Kupffer cells, liver endothelial cells, and hepatocytes.



e



f

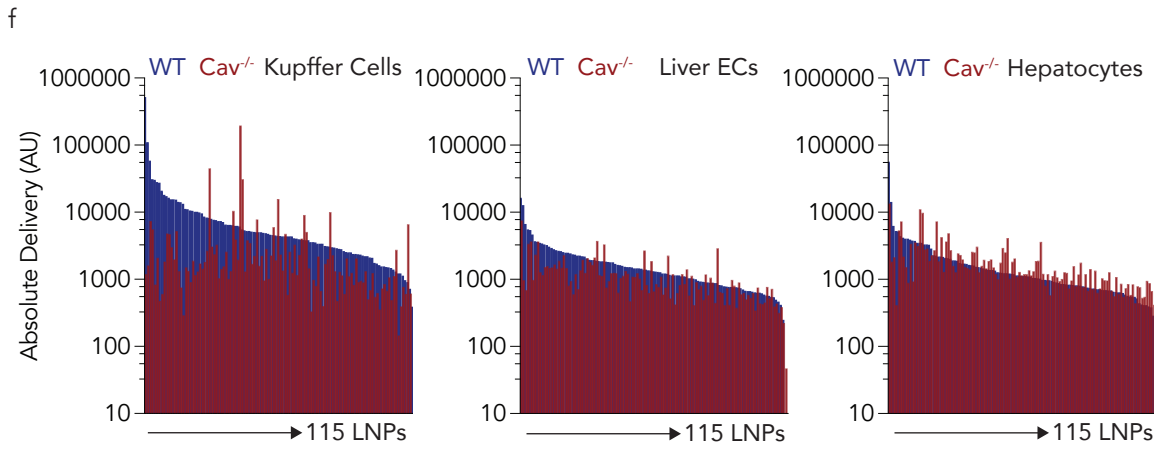


Figure S6. **(a)** Normalized nanoparticle biodistribution across two screens (226 LNPs) in liver, lung, heart, and kidney endothelial cells. **(b)** QUANT demonstrates that endothelial cells in Cav1^{-/-} uptake less QUANT barcodes than endothelial cells in wild-type mice. *p<0.05, ***p<0.001 1 tailed t-test. **(c)** Combined sequencing data and ddPCR results for each LNP in lung endothelial cells in wild type (blue) and Cav1^{-/-} (red) mice from screen 1 and screen 2 in lung, **(d)** heart, and **(e)** kidney endothelial cells.

